Materials Advances

ROYAL SOCIETY OF CHEMISTRY

PAPER

View Article Online
View Journal | View Issue

Cite this: *Mater. Adv.*, 2022, 3, 1191

H_2O_2-replenishable and GSH-depletive ROS 'bomb' for self-enhanced chemodynamic therapy†

Fan Zhao,[ab] Jiayu Yao,[c] Yu Tong,[c] Dan Su,[d] Qing Xu,[ab] Yao Ying,[ab] Wangchang Li,[ab] Juan Li,[ab] Jingwu Zheng,[ab] Liang Qiao,[ab] Wei Cai,[ab] Xiaozhou Mou,*[c] Shenglei Che,*[ab] Jing Yu*[ab] and Yanglong Hou[e]

Chemodynamic therapy (CDT) is an emerging strategy of tumor therapy that utilizes the Fenton reagent to kill tumor cells by disproportionation of H_2O_2 into hydroxyl radical (•OH). However, insufficient endogenous H_2O_2 confines the antitumor efficacy of CDT. Additionally, the overexpressed glutathione (GSH) exhibits a potent scavenging effect on cytotoxic •OH, which further diminishes the efficacy of CDT. Though tremendous efforts have been done, engineering CDT agents with efficient and specific H_2O_2 self-supplying and GSH-depletion is promising but remains a great challenge. Herein, Fe^{3+}–chelated CaO_2 nanoparticles (CaO_2–Fe NPs) are constructed as ROS 'bomb'. In the tumor microenvironment, CaO_2–Fe NPs can release Fe^{2+} by the reduction of GSH, and the remaining CaO_2 reacts with H^+ to selectively generate H_2O_2. The generated H_2O_2 can produce •OH under the catalysis of Fe^{2+} through the Fenton reaction, and re-oxidation from Fe^{2+} to Fe^{3+} endowing a long-lasting GSH-depletion, resulting in an improved CDT. These CaO_2–Fe NPs supply H_2O_2 and exhaust GSH simultaneously to achieve a self-enhanced CDT, and paves an emerging strategy to enhance the therapeutic efficacy of CDT by combining H_2O_2-replenishable and GSH-depletive together and realizing a self-enhanced Fenton reaction cycle.

Received 26th July 2021,
Accepted 21st November 2021

DOI: 10.1039/d1ma00646k

rsc.li/materials-advances

Introduction

Reactive oxygen species (ROS) based tumor therapy is an emerging therapeutic strategy to effectively induce tumor-cell apoptosis.[1–3] Among various ROS, cytotoxic hydroxyl radical (•OH), which could be generated by H_2O_2 *via* the Fenton reaction in an acidic environment is the most destructive and commonly applied type, which is defined as chemodynamic therapy (CDT).[4–7] Benefiting from the overproduction of H_2O_2 in tumors (100 μM–1 mM) than normal tissues, and the mild acidity of the tumor microenvironment (TME), CDT is regarded as a promising method for selective-tumor therapy with the help of catalysis by ferrous ions (Fe^{2+}), manganese ions (Mn^{2+}), or cuprous ions (Cu^+).[8–11] However, some works recently suggested that the endogenous H_2O_2 in the tumor site is still insufficient to support effective CDT, which restricts the clinical application.[12–15] Therefore, the introduction of the H_2O_2-replenishable agents should be taken into consideration.

A few signs of progress have been made to increase the intratumoral H_2O_2 concentration by applying natural bio-enzymes such as glucose oxidase (GOx), nicotinamide adenine dinucleotide phosphate oxidase (NOX), and superoxide dismutase (SOD).[16–18] Nevertheless, these natural enzyme-based H_2O_2 supplements suffer from some potential issues, such as instability of biological activity, high cost, and reliance on the exogenous H_2O_2-precursors such as glucose, superoxide anion ($O_2^{\bullet-}$) or O_2.[19,20] Encouragingly, it has been reported that inexpensive calcium peroxide (CaO_2) can steadily liberate a substantial amount of H_2O_2 under acidic conditions due to the presence of peroxy bond (–O–O–), and the production of H_2O_2 based on CaO_2 is independent of additional precursors.[21–25] Thus, based on the acidic environment of the tumor, CaO_2 is a practicable H_2O_2-replenishable 'bomb' for CDT to efficiently accumulate H_2O_2 with tumor specificity.

Conceivably, if •OH generated is eliminated by ROS scavengers such as glutathione (GSH), it is worth nothing. For this reason, efficient ROS generation in the tumor runs into the

[a] *College of Materials Science and Engineering, Zhejiang University of Technology, Hangzhou 310014, China. E-mail: yujing@zjut.edu.cn, cheshenglei@zjut.edu.cn*
[b] *Research Center of Magnetic and Electronic Materials, Zhejiang University of Technology, Hangzhou 310014, China*
[c] *Hepatobiliary and Pancreatic Surgery, Key Laboratory of Tumor Molecular Diagnosis and Individualized Medicine of Zhejiang Province, Zhejiang Provincial People's Hospital, Affiliated People's Hospital of Hangzhou Medical College, Hangzhou 310014, China. E-mail: mouxz@zju.edu.cn*
[d] *Department of Oncology, Zhejiang Provincial People's Hospital, Hangzhou 310014, China*
[e] *Beijing Key Laboratory for Magnetoelectric Materials and Devices (BKL-MMD), Beijing Innovation Center for Engineering Science and Advanced Technology (BIC-ESAT), Department of Materials Science and Engineering College of Engineering, Peking University, Beijing 100871, China*

† Electronic supplementary information (ESI) available: Supplementary figures and discussions. See DOI: 10.1039/d1ma00646k

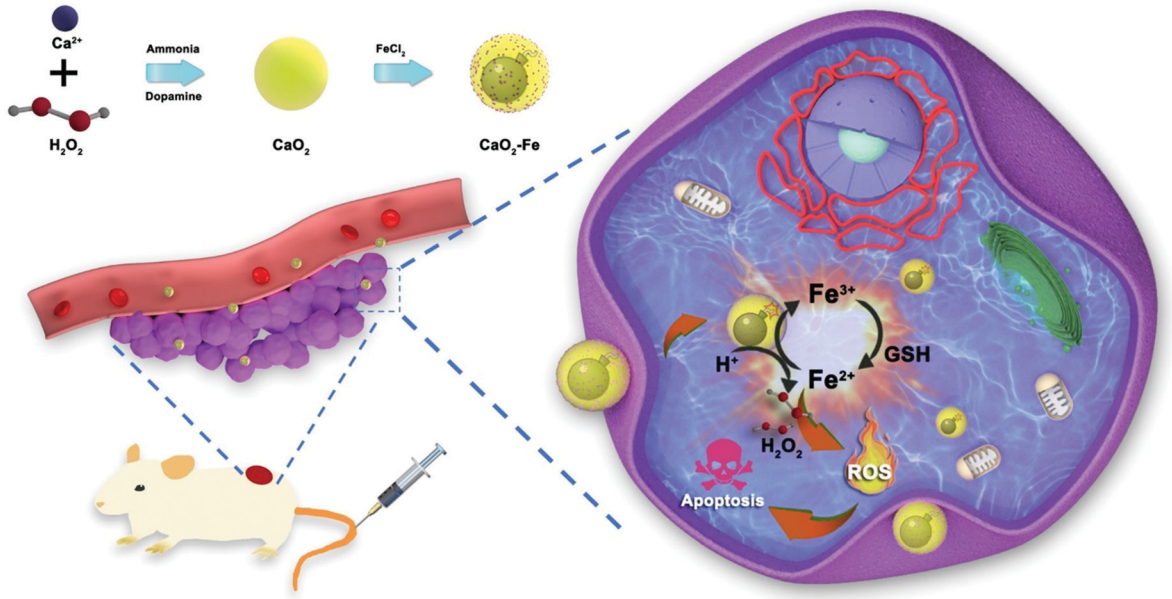

Fig. 1 The schematic illustration of CaO_2–Fe NPs as H_2O_2-replenishable and GSH-depletive ROS 'bomb' for self-enhanced CDT of the tumor.

bottleneck due to elevated GSH level intratumorally (up to 10 mM) compared with that in normal tissue.[14,26–28] This problem could be potentially solved by employing some transition metal ions with variable valences, such as ions of iron, copper, and manganese, as recyclable GSH consumers. The transformation from a high-valence ion to its low-valence form reduces the concentration of GSH, and the resulting low-valence ion is a good catalyst for the Fenton reaction.[29–31] Noteworthy that during the Fenton reaction, the low-valence ion is re-oxidized to its high-valence form, giving a sustained depletion of GSH and release of $^{\bullet}OH$ in GSH and H_2O_2-rich area.

Herein, a tumor-selective self-enhanced CDT 'bomb' is designed by using ferric ions (Fe^{3+})–chelated CaO_2 nanoparticles (CaO_2–Fe NPs). As elucidated in Fig. 1, under the tumor microenvironment, CaO_2 NPs reacted with specific H^+ to form H_2O_2 *in situ* as ROS 'bomb', and the chelated Fe^{3+} is reduced to Fe^{2+} by high-leveled GSH as the trigger. Subsequently, the Fenton reaction is activated by the generated H_2O_2 and Fe^{2+}. Finally, $^{\bullet}OH$ is produced for tumor therapy. Furthermore, the consumption of GSH enhances the CDT efficiency, and the re-oxidation of Fe^{2+} to Fe^{3+} endowing a long-lasting GSH-depletion. As a result, CaO_2–Fe NPs are able to selectively generate amounts of ROS to induce apoptosis of tumor cells with low systemic toxicity both *in vitro* and *in vivo*. These CaO_2–Fe NPs are good candidates for constructing ROS 'bomb' with endogenous replenishment of H_2O_2 and depletion of GSH, providing a novel strategy for improving tumor-selective CDT.

Results and discussion

To obtain CaO_2–Fe NPs, CaO_2 NPs were first synthesized *via* a modified dopamine-assisted method, followed by mixing ferrous chloride to load iron ions.[21,32,33] The chelated iron contents were adjusted by different feeding ratios between CaO_2 and ferrous chloride (mass ratio). As shown in Table S1 (ESI†), contents of the chelated iron within CaO_2-Fe NPs were gradually improved with the increase of the feeding ratio. However, CaO_2–Fe NPs would not be formed when the feeding ratios were higher than 2 : 1. Thus, feeding ratios (4 : 1) were chosen to synthesize CaO_2–Fe NPs. The morphology of CaO_2–Fe NPs remained unchanged compared with the original CaO_2 NPs, and their diameters increased from 91 nm to 122 nm (Fig. 2a and Fig. S1, S2, ESI†). Subsequently, as confirmed using X-ray diffraction (XRD), the introduction of iron ions could not influence the phase of CaO_2 NPs (Fig. 2b). Strong and homogeneous iron signals were then observed from energy-dispersive X-ray spectroscopy (EDS) and EDS mapping, demonstrating the efficient binding of iron ions within CaO_2 NPs (Fig. 2c and Fig. S3, ESI†). To explore the valence state of chelated iron ions, X-ray photoelectron spectrometry (XPS) was applied. The central peak at ~710.0 eV (Fe $2p_{3/2}$) and the shakeup satellite peak at ~724.0 eV (Fe $2p_{1/2}$) demonstrated that Fe^{2+} was transformed into Fe^{3+}, which might be oxidized by CaO_2 (Fig. 2d and e). The photoelectron peak at 532.5 eV of O 1s could be assigned to O–O, indicating the presence of peroxo groups (Fig. 2f).[24]

Considering the significance of H_2O_2 for CDT, the H_2O_2 generation ability of CaO_2–Fe NPs was investigated using potassium permanganate ($KMnO_4$) as the indicator. As shown in Fig. 3a, the color of permanganate (MnO_4^-) disappeared after adding CaO_2–Fe NPs to the acidic solution, suggesting the reduction of MnO_4^- to colorless Mn^{2+} by the generated H_2O_2. The dissociation of CaO_2–Fe NPs in acidic solution further verified the acid-activated H_2O_2 generation (Fig. S4, ESI†). In comparison, less H_2O_2 was generated from CaO_2–Fe NPs in a

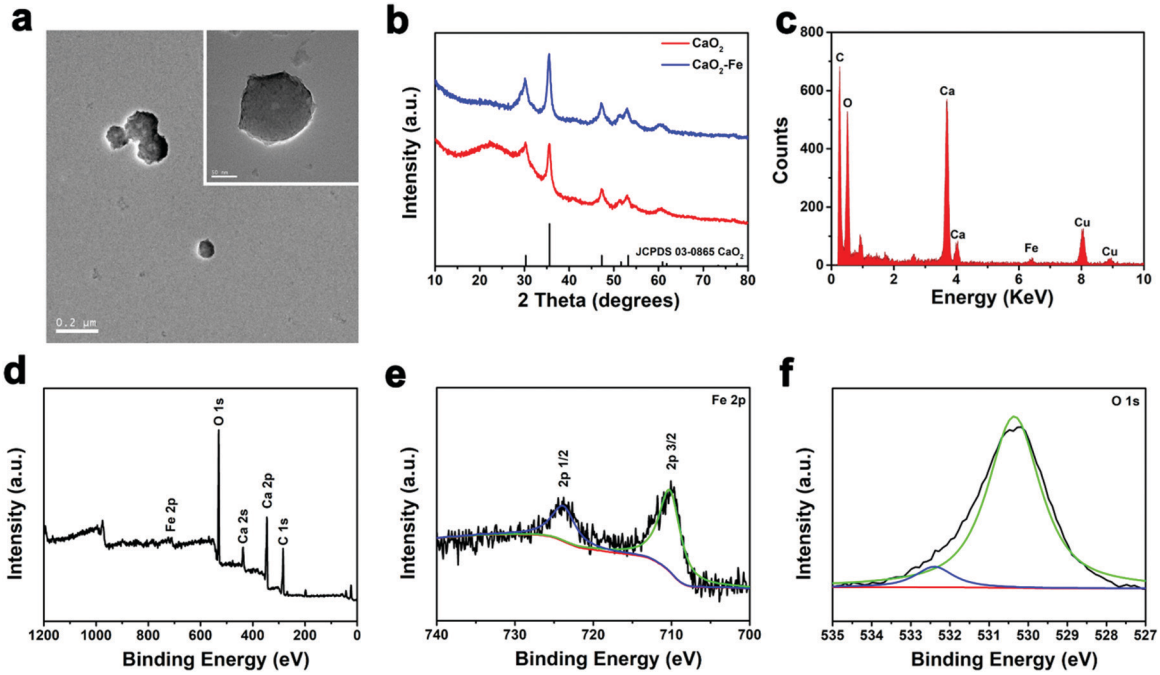

Fig. 2 (a) TEM image of CaO_2–Fe nanoparticles (inset: an image at a higher magnification of CaO_2–Fe NPs). (b) XRD pattern of CaO_2 and CaO_2–Fe NPs. (c) EDS spectrum of CaO_2–Fe NPs. (d) Survey XPS spectra of CaO_2–Fe NPs. (e) High-resolution Fe 2p XPS spectra of CaO_2–Fe NPs. (f) High-resolution O 1s XPS spectra of CaO_2–Fe NPs.

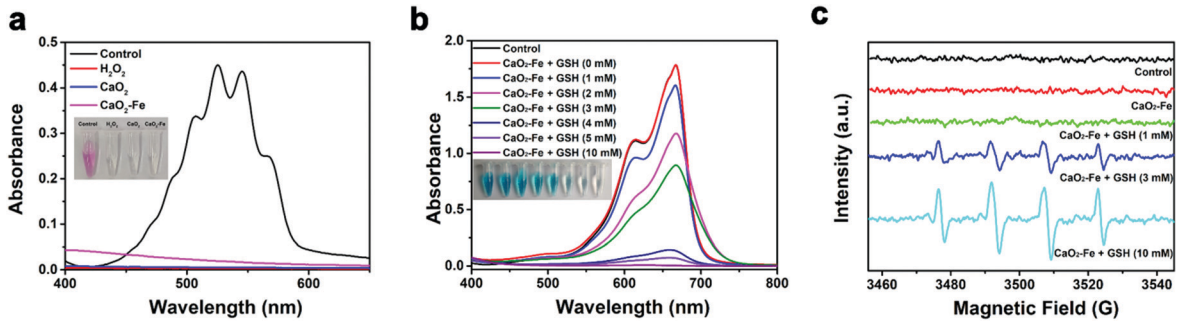

Fig. 3 (a) UV-Vis absorption spectra and photo (inset) of $KMnO_4$ after treating with H_2O_2, CaO_2 NPs, and CaO_2–Fe NPs in an acidic environment. (b) UV-vis absorption spectra and photo (inset) of MB after degradation by CaO_2–Fe NPs treated with different amounts of GSH at pH 5.4. (c) ESR spectra of CaO_2–Fe NPs treated with different amounts of GSH at pH 5.4 (5,5-dimethyl-1-pyrroline N-oxide (DMPO) as the spin trap).

neutral environment (Fig. S5, ESI†). CaO_2–Fe NPs could maintain long-term stability in a neutral environment (Fig. S6, ESI†). It indicated that CaO_2–Fe NPs were good candidates for H_2O_2-replenishment in the acidic environment. These H_2O_2 suppliers could further release $^{\bullet}OH$ induced by the Fenton reaction.

To evaluate the ROS triggered by CaO_2–Fe NPs, methylene blue (MB) was selected as the indicator. As can be seen in Fig. 3b and Fig. S7, S8 (ESI†), GSH is essential for ROS generation based on CaO_2–Fe NPs, due to the generation of Fenton-catalytic Fe^{2+} by the reduction of GSH. It is noteworthy that a high level of GSH was adverse for ROS generation in most reported cases due to the strong scavenging effect of GSH on ROS.[14,26] While CaO_2–Fe NPs exhibited an excellent ROS releasing capacity even when the concentration of GSH was at 10 mM, with the MB degradation efficiency appeared to be 99%. This phenomenon could be ascribed to the continuous depletion of GSH under the Fenton reaction cycle based on CaO_2–Fe NPs (Fig. S9, ESI†). During the GSH depletion and Fenton reaction cycle, Fe^{3+} was indispensable. In comparison with bare CaO_2 NPs without Fe^{3+} chelated, CaO_2–Fe NPs showed enhanced degradation of MB (Fig. S10, ESI†). Moreover, the ROS generation ability of CaO_2–Fe NPs was increased with the improvement of the chelated iron content (Fig. S11, ESI†). In addition, CaO_2–Fe NPs also showed a pH-dependent ROS due to the reliance on the generation of acidity of H_2O_2. These CaO_2–Fe NPs caused an apparent color degradation of MB under acidic conditions (pH 5.4) with the the assistance of GSH, but no significant change was observed under neutral conditions

(pH 7.4) (Fig. S12, ESI†). The type of ROS produced by CaO_2–Fe NPs was further verified by the electron paramagnetic resonance (EPR) spin-trapping method. As shown in Fig. 3c, a characteristic 1 : 2 : 2 : 1 signal was obtained, indicating that the produced ROS by CaO_2–Fe NPs was •OH. These results suggested that CaO_2–Fe NPs were promising candidates for pH/GSH dual stimuli-activated CDT agents by H_2O_2 self-supplying and GSH-depletion.

Encouraged by the efficient production of •OH *via* CaO_2–Fe NPs with the assistance of GSH and H^+, *in vitro* •OH generation was investigated due to the higher intracellular GSH concentration and lower pH value in tumor cells. By employing 2,7-dichlorofluorescin diacetate (DCFH-DA) as the •OH indicator, fluorescence imaging was carried out on 4T1 cells, which showed that the fluorescence signal of CaO_2–Fe NPs was dosage-dependent (Fig. S13, ESI†). Compared with CaO_2 NPs and $FeCl_3$ at the same dosage, CaO_2–Fe NPs exhibited significantly stronger green fluorescence, indicating the self-enhanced •OH was generated from CaO_2–Fe NPs in tumor cells (Fig. 4a and Fig. S14, ESI†). Considering the therapeutic effect of •OH, cell viability was then investigated by standard methyl thiazolyl tetrazolium (MTT) assay. As shown in Fig. 4b, CaO_2–Fe NPs induced greater cell death by increasing concentrations, and the cytotoxic effect of the CaO_2–Fe NPs treated group was greater than that of $FeCl_3$ and CaO_2 NPs at the same concentration. Results from live/dead cell staining assay further confirmed these results, which revealed that only a small number of 4T1 cells remained viable after treatment with CaO_2–Fe NPs, while only a few cells were dead after treatment with $FeCl_3$ and CaO_2 NPs for 24 h (Fig. 4c and Fig. S15, ESI†).

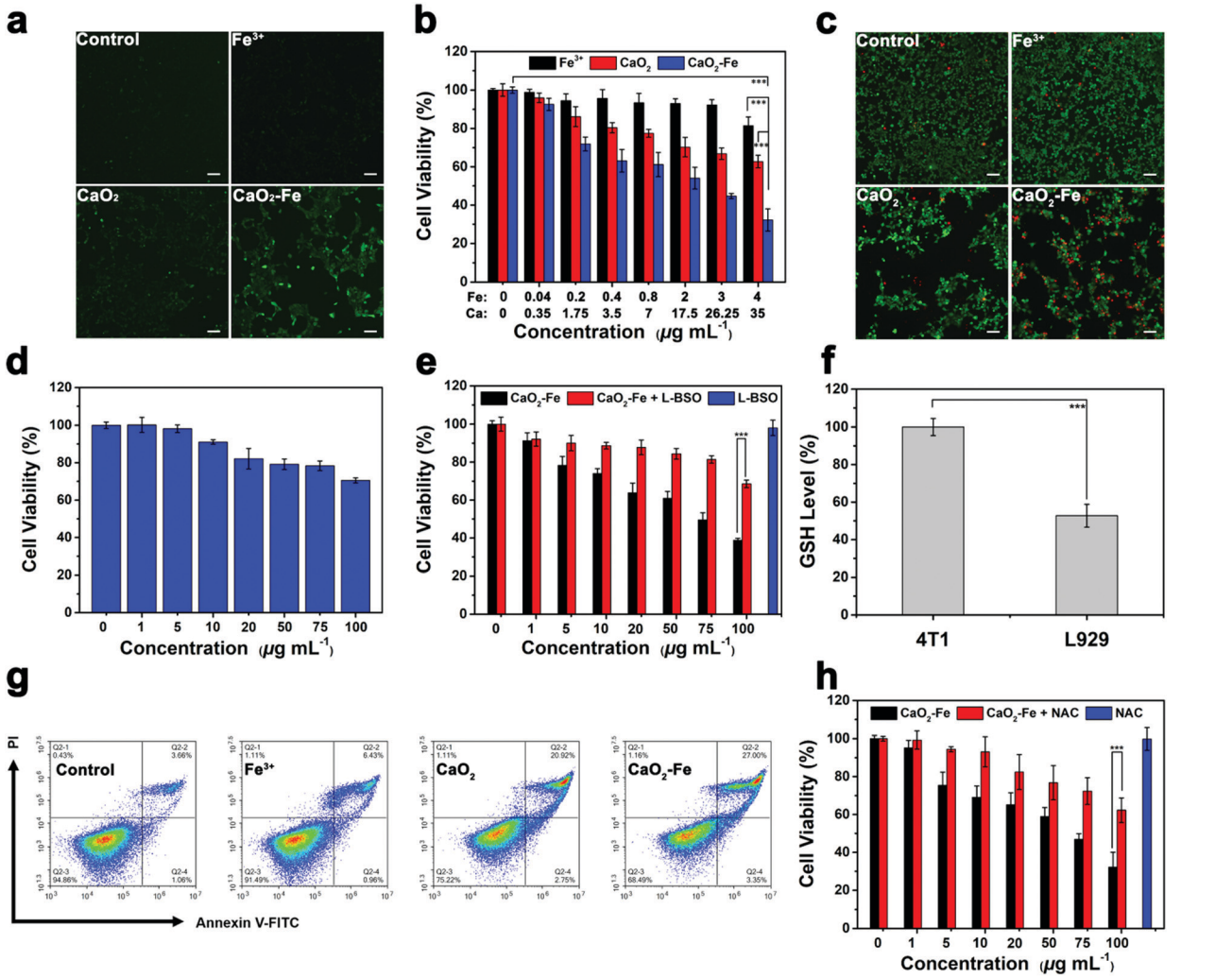

Fig. 4 (a) Fluorescence images of DCFH-DA stained 4T1 cells after exposure to $FeCl_3$, CaO_2 NPs, and CaO_2–Fe NPs for 4 h. The scale bar represents 100 μm. (b) Viability of 4T1 cells after 24 h of incubation with $FeCl_3$, CaO_2 NPs, and CaO_2–Fe NPs. (n = 6, mean ± s.d., ***$p < 0.001$) (c) Fluorescence images of Calcein AM (green, live cells) and PI (red, dead cells) costained 4T1 cells after incubation with $FeCl_3$, CaO_2 NPs, and CaO_2–Fe NPs for 24 h. The scale bar represents 100 μm. (d) Viability of L929 cells after 24 h of incubation with CaO_2–Fe NPs. (n = 6, mean ± s.d.) (e) Viability of 4T1 cells after 24 h of incubation with CaO_2–Fe NPs plus or without L-BSO. (n = 6, mean ± s.d., ***$p < 0.001$) (f) Intracellular GSH levels of 4T1 cells and L929 cells. (n = 3, mean ± s.d., ***$p < 0.001$) (g) Flow cytometry analysis of 4T1 cells treated with $FeCl_3$, CaO_2 NPs, and CaO_2–Fe NPs for 24 h. (h) Viability of 4T1 cells after 24 h of incubation with CaO_2–Fe NPs plus or without NAC. (n = 6, mean ± s.d., ***$p < 0.001$).

Interestingly, the cell inhibition effect from CaO_2–Fe NPs was tumor cell-selective toxicity, which presented relatively low cytotoxicity toward normal cells (Fig. 4d and Fig. S16, ESI†). This phenomenon could be ascribed to the reliance of $^{\bullet}OH$ generation on GSH concentration (Fig. 4e and Fig. S17, ESI†). After treating with CaO_2–Fe NPs, the intracellular GSH level was decreased, and the cell viability was reversed by down-regulating GSH by using L-buthionine sulfoximine (L-BSO) as the GSH inhibitor. In addition, GSH concentration within normal cells (L929) was much lower than cancerous cells (4T1) (Fig. 4f). As a result, reduced GSH could hardly trigger the generation of enough $^{\bullet}OH$ on normal cells (Fig. S18, ESI†), and finally suppressed the side effect.

Flow cytometry was further used to investigate the type of cell death using the annexin V-FITC/PI detection kit. As shown in Fig. 4g, cell death induced by all groups was apoptosis, and the CaO_2–Fe NPs treated group had higher ratios of apoptotic cells (27%) than other groups. As ROS-mediated cell killing is regarded as the major pathway for apoptosis, the influence of *N*-acetyl-cysteine (NAC), a kind of ROS scavenger, on cell viability was then investigated. With the addition of NAC, cell apoptosis induced by CaO_2–Fe NPs was obviously reversed, indicating the cell inhibition was originating from the production of ROS in tumor cells (Fig. 4h). All these results suggested that CaO_2–Fe NPs was a GSH-enhanced CDT 'bomb' with self-supplied H_2O_2 to induce tumor cell apoptosis efficiently and selectively by $^{\bullet}OH$.

Tumor growth inhibition experiment was next performed by intravenous (*i.v.*) administration, inspired by outstanding treatment outcome of CaO_2–Fe NPs *in vitro*. *In vivo* biodistribution of CaO_2–Fe NPs was initially evaluated by labelling NIR dye (IR-783). As shown in Fig. S19 (ESI†), the CaO_2–Fe NPs could be accumulated in tumor tissue *via* the EPR effect, indicating that CaO_2–Fe NPs could serve as the ROS 'bomb' for self-enhanced chemodynamic therapy. The half-life of CaO_2–Fe NPs was 1.17 ± 0.45 h (Fig. S20, ESI†). Mice treated with saline (as the control group), $FeCl_3$, and CaO_2 NPs showed rapid tumor growth, while the size of tumors in CaO_2–Fe NPs injected mice was substantially inhibited (Fig. 5a and b). The therapeutic efficacy was also evidenced by hematoxylin and eosin (H&E) staining and terminal deoxynucleotidyl transferase-mediated dUTP nick-end labeling (TUNEL) staining, which revealed extensive tumor cell apoptosis after treatment with CaO_2–Fe NPs (Fig. 5c). The effective generation of toxic $^{\bullet}OH$ under TME

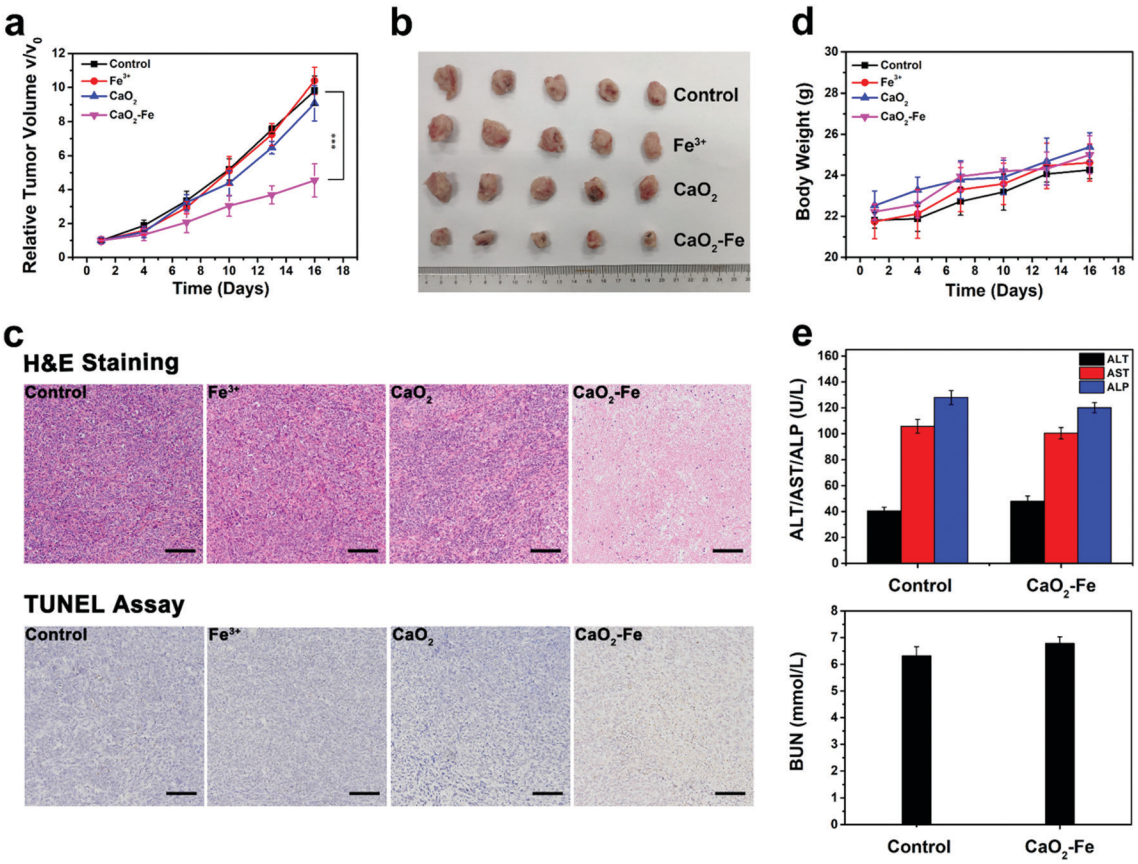

Fig. 5 (a) Relative tumor growth curves of 4T1 tumor-bearing mice after treatment with saline (control group), $FeCl_3$, CaO_2 NPs, and CaO_2–Fe NPs. (n = 5, mean ± s.d., ***$p < 0.001$) (b) A representative photo of dissected tumors from the different groups on day 17 after administration. (c) Images of H&E and TUNEL stained sections of tumors from the different groups on day 17 after administration. The scale bar represents 100 μm. (d) Time-dependent body-weight curves of mice in different groups. (n = 5, mean ± s.d.) (e) Blood biochemistry analysis of healthy mice after intravenously injected with saline or CaO_2–Fe NPs for 17 days. (n = 3, mean ± s.d.).

with acidic pH and overexpressed GSH from CaO_2–Fe NPs, leading to a remarkable tumor growth inhibition effect. Moreover, no apparent body weight changes were observed in mice injected with CaO_2–Fe NPs during the whole period (Fig. 5d), and there was no obvious histological alteration in the major organs (Fig. S21, ESI†). No obvious physiological damages were observed in CaO_2–Fe NPs treated group through blood biochemistry and hematology analysis (Fig. 5e and Fig. S22, ESI†). Therefore, it is feasible to use CaO_2–Fe NPs as a smart CDT agent for effective tumor therapy with low toxicity.

Conclusions

In summary, an H_2O_2-replenishable and GSH-depletive ROS 'bomb' was successfully constructed for self-enhanced chemodynamic tumor therapy. After reaching tumor tissues, these ROS 'bomb', CaO_2–Fe NPs, could be triggered due to the generation of Fe^{2+} ions by GSH. Meanwhile, amounts of H_2O_2 were generated by the reaction between CaO_2 and H^+. Eventually, with the accumulation of H_2O_2 as well as Fe^{2+} locally, a Fenton reaction cycle was achieved by continuously consuming GSH to output massive ROS, resulting in the improvement of the CDT efficacy by H_2O_2-supplementing and GSH-depletion. Both, *in vitro* and *in vivo* results demonstrated that CaO_2–Fe NP presented an inspiring antitumor performance as well as low systemic toxicity. Therefore, these CaO_2–Fe NPs could be regarded as a promising candidate for combining pH/GSH-responsive and GSH-depletion for CDT.

Experimental section

Materials

Calcium chloride ($CaCl_2$, 96%), ammonium hydroxide ($NH_3 \cdot H_2O$, 28%), dopamine (99%), ferrous chloride ($FeCl_2$, 98%), methylene blue (MB, 70%), *N*-acetyl cysteine (NAC), and glutathione (GSH, 99%) were obtained from J&K Scientific Ltd (Beijing, China). Ethanol (C_2H_6OH, 99.7%) and hydrogen peroxide (H_2O_2, 30%) were purchased from the Juhua Group Corporation.

Characterization

X-Ray diffraction patterns (XRD) was recorded using the X'Pert PRO X-ray diffractometer with Cu Kα (λ = 1.54 Å). Transmission electron microscopy (TEM) was performed using a FEI Tecnai G2 F30 microscope. X-Ray photoelectron spectroscopy (XPS) was performed using the Axis Ultra imaging photoelectron spectrometer (Kratos Analytical Ltd). Dynamic light scattering (DLS) measurements were conducted using the Zetasizer Nano ZS (Malvern). The concentrations of Fe and Ca were quantified using an inductively coupled plasma-atomic emission spectrometer (ICP-AES, NexION 350, PerkinElmer).

Synthesis of CaO_2 NPs and CaO_2–Fe NPs

$CaCl_2$ (0.1 g) and dopamine (0.003 g) were first dissolved in ethanol (15 mL) with the help of ultrasound. Subsequently, NH_4OH (1 mL) was added under magnetic stirring. Afterwards, H_2O_2 solution (0.2 mL) was injected slowly. The product (CaO_2 NPs) was finally collected by centrifugation (8000 rpm), washed with ethanol three times, and redispersed in ethanol. CaO_2 NPs were then reacted with $FeCl_2$ to form CaO_2–Fe NPs.

Colorimetric assay of peroxo groups

An aqueous solution containing $KMnO_4$ (50 μg mL^{-1}) and HCl (0.1 M) was first prepared. Subsequently, a certain amount of CaO_2 NPs, CaO_2–Fe NPs, or H_2O_2 was added into the mixture for 5 min. Finally, the mixture was measured by UV-vis spectra.

Chemodynamic activity of CaO_2–Fe NPs

The degradation of methylene blue (MB) was used for quantitative analysis of ROS production based on CaO_2–Fe NPs. In particular, the absorbance at λ = 644 nm of MB solution (25 mg L^{-1}) in pH 7.4 or pH 5.4 with or without different concentrations of GSH (0, 1, 2, 3, 4, 5, and 10 mM) was measured before and after adding of 20 μg CaO_2 NPs or CaO_2–Fe NPs for 3 hours.

To confirm the ROS type from CaO_2–Fe NPs, ESR spectroscopy was used. 5,5-Dimethyl-1-pyrroline N-oxide (DMPO) was utilized as the spin trap. DMPO solution (40 μL, 100 mmol L^{-1}) was added into CaO_2–Fe NP solution at different concentrations of GSH (0, 1, 3, and 10 mM) at pH 5.4. Subsequently, the above mixture (20 μL) was injected into a capillary, the results were recorded using a Bruker A300.

Cell culture

4T1 and L929 cell lines were obtained from Zhejiang Provincial People's Hospital. All biological reagents were purchased from Biological Industries. DMEM or 1640 with 10% FBS and 1% penicillin/streptomycin were treated as the cell culture medium. All cells were cultured in a cell incubator at 37 °C, 5% CO_2 and 100% humidity.

Cytotoxicity assays

MTT assay was tested to evaluate the *in vitro* cytotoxicity. First, 5×10^3 per well 4T1 and L929 cells were seeded into 96-well plates and incubated overnight. Subsequently, various amounts of $FeCl_3$, CaO_2 NPs, and CaO_2–Fe NPs at the same Ca or Fe concentrations were added. After further incubation for 24 h, a fresh cell culture medium with 5% 3-[4,5-dimethylthiazol-2-yl-]-2,5-diphenyltetrazolium bromide (MTT) was used to replace the culture medium with nanoparticles. Finally, dimethyl sulfoxide (DMSO, 100 μL) was used to replace the MTT solution and co-incubation for 4 h. Cell viability was measured using a Tecan m200. Furthermore, after 4T1 cells were treated after the above conditions, Calcein-AM and propidium iodide (PI) live/dead cell staining was used to further verify the cytotoxicity of CaO_2–Fe NPs.

Intracellular ROS levels detection

5×10^4 per well 4T1 and L929 cells were plated into a 24-well plate and incubated overnight. Then, cells were incubated with $FeCl_3$, CaO_2 NPs, and CaO_2–Fe NPs at the same Ca or Fe

concentrations for 4 h. After washing with PBS, cells were stained with DCFH-DA (10 μM) for 30 min. Later, PBS was used to remove the free DCFH-DA. Finally, the fluorescence images were obtained using a Nikon ECLIPSE Ti.

Assessment of apoptosis

Annexin-V/PI assay kit (Sony) was used to determine the apoptosis of 4T1 cells treated with CaO_2–Fe NPs using flow cytometry. In particular, 2×10^5 per well 4T1 cells were plated into a 6-well plate and incubated for 12 h. Afterwards, cells were treated with $FeCl_3$, CaO_2 NPs, and CaO_2–Fe NPs at the same Ca or Fe concentrations for a further 24 h. After washing with PBS, cells were detached by trypsin. Finally, apoptosis was detected using flow cytometry (ACEA NovoCyte) using PI *vs.* Annexin V plots.

Animal modal

All animal experiments were performed abiding by the guidelines of the Institutional Animal Care and Use Committee (IACUC) of Zhejiang Provincial People's Hospital, Hangzhou, China. 6-Week female Balb/c mice were provided by Shanghai Sippe-Bk Lab Animal Co., Ltd, Shanghai, China. 1×10^6 4T1 cells solution (0.1 mL cells in PBS) was subcutaneously injected into the right axillary of all mice to construct the tumor model.

Tumor inhibition and *in vivo* toxicity assay

After tumor volume reached 100 mm^3, 20 mice were randomly divided into 4 groups ($n = 5$): mice were intravenously injected with saline (as the control group), $FeCl_3$, CaO_2 NPs, and CaO_2–Fe NPs at the same Ca or Fe concentrations. The whole experiment period was 15 days. All treatments were performed every three days and tumor volume and body weight were recorded 1-day after injection. Tumor volume was calculated using the formula as $0.5 \times (\text{length} \times \text{width}^2)$.

On the 17th day, all mice were executed. Subsequently, tumors and major organs (heart, liver, spleen, lung, and kidney) were removed and stored in formalin. After the section of the tumors and major organs, hematoxylin and eosin (H&E) staining and terminal deoxynucleotidyl transferase-mediated dUTP nick-end labeling (TUNEL) staining were then detected. A Nikon ECLIPSE Ni-U was used to observe the slides.

Statistical analysis

The test data are shown as mean ± s.d. The student's two-tailed *t*-test was used to calculate the statistical comparisons. * means $p < 0.05$, ** means $p < 0.01$, *** means $p < 0.001$. $p < 0.05$ was regarded as statistically significant.

Author contributions

Fan Zhao: carried out all experiments and performed the statistical analysis, contributed to discussion, writing – original draft. Jiayu Yao: participated in animal studies and molecular biology experiments. Yu Tong: participated in animal studies and molecular biology experiments. Qing Xu: participated in molecular biology experiments. Dan Su: participated in molecular biology experiments. Juan Li: supervision. Yao Ying: supervision. Wangchang Li: supervision. Liang Qiao: supervision. Jingwu Zheng: supervision. Wei Cai: supervision. Xiaozhou Mou: conceptualization, supervision, writing – reviewing and editing. Shenglei Che: conceptualization, supervision, writing – reviewing and editing. Jing Yu: carried out all experiments and performed the statistical analysis, conceptualization, writing – review & editing. Yanglong Hou: conceptualization, supervision, writing – reviewing and editing.

Conflicts of interest

There are no conflicts to declare.

Acknowledgements

This work was supported in part by the National Natural Science Foundation of China (52073258 and 81672430), Natural Science Foundation of Zhejiang Province (LY20E020017 and LQ19H160016), Young Elite Scientist Sponsorship Program by CAST (2017QNRC001), the Fundamental Research Funds for the Provincial Universities of Zhejiang (RF-A2019004), and Foundation of Health Department of Zhejiang Province (2018KY239).

References

1 C. Li, X. Zheng, W. Chen, S. Ji, Y. Yuan and X. Jiang, Tumor microenvironment-regulated and reported nanoparticles for overcoming the self-confinement of multiple photodynamic therapy, *Nano Lett.*, 2020, **20**, 6526–6534.
2 Y. Chen, Y. Huang, S. Zhou, M. Sun, L. Chen, J. Wang, M. Xu, S. Liu, K. Liang, Q. Zhang, T. Jiang, Q. Song, G. Jiang, X. Tang, X. Gao and J. Chen, Tailored chemodynamic nanomedicine improves pancreatic cancer treatment via controllable damaging neoplastic cells and reprogramming tumor microenvironment, *Nano Lett.*, 2020, **20**, 6780–6790.
3 V. G. Deepagan, D. G. You, W. Um, H. Ko, S. Kwon, K. Y. Choi, G.-R. Yi, J. Y. Lee, D. S. Lee, K. Kim, I. C. Kwon and J. H. Park, Long-circulating Au-TiO_2 nanocomposite as a sonosensitizer for ROS-mediated eradication of cancer, *Nano Lett.*, 2016, **16**, 6257–6264.
4 H. Ranji-Burachaloo, P. A. Gurr, D. E. Dunstan and G. G. Qiao, Cancer treatment through nanoparticle-facilitated Fenton reaction, *ACS Nano*, 2018, **12**, 11819–11837.
5 M. Wu, Y. Ding and L. Li, Recent progress in the augmentation of reactive species with nanoplatforms for cancer therapy, *Nanoscale*, 2019, **11**, 19658–19683.
6 Y. Wang, L. Shi, Z. Ye, K. Guan, L. Teng, J. Wu, X. Yin, G. Song and X. Zhang, Reactive oxygen correlated chemiluminescent imaging of a semiconducting polymer nanoplatform for monitoring chemodynamic therapy, *Nano Lett.*, 2020, **20**, 176–183.

7 C. Zhang, W. Bu, D. Ni, S. Zhang, Q. Li, Z. Yao, J. Zhang, H. Yao, Z. Wang and J. Shi, Synthesis of iron nanometallic glasses and their application in cancer therapy by a localized Fenton reaction, *Angew. Chem., Int. Ed.*, 2016, **55**, 2101–2106.

8 C. Wu, S. Wang, J. Zhao, Y. Liu, Y. Zheng, Y. Luo, C. Ye, M. Huang and H. Chen, Biodegradable Fe(III)@WS_2-PVP nanocapsules for redox reaction and tme-enhanced nanocatalytic, photothermal, and chemotherapy, *Adv. Funct. Mater.*, 2019, **29**, 1901722.

9 L. Zhang, S. Wan, C.-X. Li, L. Xu, H. Cheng and X. Zhang, An adenosine triphosphate-responsive autocatalytic Fenton nanoparticle for tumor ablation with self-supplied H_2O_2 and acceleration of Fe(III)/Fe(II) conversion, *Nano Lett.*, 2018, **18**, 7609–7618.

10 X. Chen, H. Zhang, M. Zhang, P. Zhao, R. Song, T. Gong, Y. Liu, X. He, K. Zhao and W. Bu, Amorphous Fe-based nanoagents for self-enhanced chemodynamic therapy by re-establishing tumor acidosis, *Adv. Funct. Mater.*, 2020, **30**, 1908365.

11 J. Yu, F. Zhao, W. Gao, X. Yang, Y. Ju, L. Zhao, W. Guo, J. Xie, X.-J. Liang, X. Tao, J. Li, Y. Ying, W. Li, J. Zheng, L. Qiao, S. Xiong, X. Mou, S. Che and Y. Hou, Magnetic reactive oxygen species nanoreactor for switchable magnetic resonance imaging guided cancer therapy based on pH-sensitive Fe_5C_2@Fe_3O_4 nanoparticles, *ACS Nano*, 2019, **13**, 10002–10014.

12 X. Qian, J. Zhang, Z. Gu and Y. Chen, Nanocatalysts-augmented Fenton chemical reaction for nanocatalytic tumor therapy, *Biomaterials*, 2019, **211**, 1–13.

13 M. Wu, Y. Ding and L. Li, Recent progress in the augmentation of reactive species with nanoplatforms for cancer therapy, *Nanoscale*, 2019, **11**, 19658–19683.

14 L.-S. Lin, J. Song, L. Song, K. Ke, Y. Liu, Z. Zhou, Z. Shen, J. Li, Z. Yang, W. Tang, G. Niu, H.-H. Yang and X. Chen, Simultaneous Fenton-like ion delivery and glutathione depletion by MnO_2-based nanoagent to enhance chemodynamic therapy, *Angew. Chem., Int. Ed.*, 2018, **57**, 4902–4906.

15 X. Wang, F. Li, X. Yan, Y. Ma, Z.-H. Miao, L. Dong, H. Chen, Y. Lu and Z. Zha, Ambient aqueous synthesis of ultrasmall Ni0.85Se nanoparticles for noninvasive photoacoustic imaging and combined photothermal-chemotherapy of cancer, *ACS Appl. Mater. Interfaces*, 2017, **9**, 41782–41793.

16 P. a. Ma, H. Xiao, C. Yu, J. Liu, Z. Cheng, H. Song, X. Zhang, C. Li, J. Wang, Z. Gu and J. Lin, Enhanced cisplatin chemotherapy by iron oxide nanocarrier-mediated generation of highly toxic reactive oxygen species, *Nano Lett.*, 2017, **17**, 928–937.

17 M. Huo, L. Wang, Y. Chen and J. Shi, Tumor-selective catalytic nanomedicine by nanocatalyst delivery, *Nat. Commun.*, 2017, **8**, 357.

18 L.-H. Fu, C. Qi, Y.-R. Hu, J. Lin and P. Huang, Glucose oxidase-instructed multimodal synergistic cancer therapy, *Adv. Mater.*, 2019, **31**, 1808325.

19 L.-H. Fu, C. Qi, J. Lin and P. Huang, Catalytic chemistry of glucose oxidase in cancer diagnosis and treatment, *Chem. Soc. Rev.*, 2018, **47**, 6454–6472.

20 Y. Dai, Z. Yang, S. Cheng, Z. Wang, R. Zhang, G. Zhu, Z. Wang, B. C. Yung, R. Tian, O. Jacobson, C. Xu, Q. Ni, J. Song, X. Sun, G. Niu and X. Chen, Toxic reactive oxygen species enhanced synergistic combination therapy by self-assembled metal-phenolic network nanoparticles, *Adv. Mater.*, 2018, **30**, 1704877.

21 S. Shen, M. Mamat, S. Zhang, J. Cao, Z. D. Hood, L. Figueroa-Cosme and Y. Xia, Synthesis of CaO_2 nanocrystals and their spherical aggregates with uniform sizes for use as a biodegradable bacteriostatic agent, *Small*, 2019, **15**, 1902118.

22 M. Zhang, R. Song, Y. Liu, Z. Yi, X. Meng, J. Zhang, Z. Tang, Z. Yao, Y. Liu, X. Liu and W. Bu, Calcium-overload-mediated tumor therapy by calcium peroxide nanoparticles, *Chem*, 2019, **5**, 2171–2182.

23 S. Gao, Y. Jin, K. Ge, Z. Li, H. Liu, X. Dai, Y. Zhang, S. Chen, X. Liang and J. Zhang, Self-supply of O_2 and H_2O_2 by a nanocatalytic medicine to enhance combined chemo/chemodynamic therapy, *Adv. Sci.*, 2019, **6**, 1902137.

24 L.-S. Lin, T. Huang, J. Song, X.-Y. Ou, Z. Wang, H. Deng, R. Tian, Y. Liu, J.-F. Wang, Y. Liu, G. Yu, Z. Zhou, S. Wang, G. Niu, H.-H. Yang and X. Chen, Synthesis of copper peroxide nanodots for H_2O_2 self-supplying chemodynamic therapy, *J. Am. Chem. Soc.*, 2019, **141**, 9937–9945.

25 Z. Tang, Y. Liu, D. Ni, J. Zhou, M. Zhang, P. Zhao, B. Lv, H. Wang, D. Jin and W. Bu, Biodegradable nanoprodrugs: "Delivering" ROS to cancer cells for molecular dynamic therapy, *Adv. Mater.*, 2020, **32**, 1904011.

26 C. Liu, D. Wang, S. Zhang, Y. Cheng, F. Yang, Y. Xing, T. Xu, H. Dong and X. Zhang, Biodegradable biomimic copper/manganese silicate nanospheres for chemodynamic/photodynamic synergistic therapy with simultaneous glutathione depletion and hypoxia relief, *ACS Nano*, 2019, **13**, 4267–4277.

27 F. Gong, L. Cheng, N. Yang, O. Betzer, L. Feng, Q. Zhou, Y. Li, R. Chen, R. Popovtzer and Z. Liu, Ultrasmall oxygen-deficient bimetallic oxide $MnWO_X$ nanoparticles for depletion of endogenous gsh and enhanced sonodynamic cancer therapy, *Adv. Mater.*, 2019, **31**, 1900730.

28 G. Chen, Y. Yang, Q. Xu, M. Ling, H. Lin, W. Ma, R. Sun, Y. Xu, X. Liu, N. Li, Z. Yu and M. Yu, Self-amplification of tumor oxidative stress with degradable metallic complexes for synergistic cascade tumor therapy, *Nano Lett.*, 2020, **20**, 8141–8150.

29 Y. Liu, W. Zhen, L. Jin, S. Zhang, G. Sun, T. Zhang, X. Xu, S. Song, Y. Wang, J. Liu and H. Zhang, All-in-one theranostic nanoagent with enhanced reactive oxygen species generation and modulating tumor microenvironment ability for effective tumor eradication, *ACS Nano*, 2018, **12**, 4886–4893.

30 B. Ma, S. Wang, F. Liu, S. Zhang, J. Duan, Z. Li, Y. Kong, Y. Sang, H. Liu, W. Bu and L. Li, Self-assembled copper-amino acid nanoparticles for in situ glutathione "AND" H_2O_2 sequentially triggered chemodynamic therapy, *J. Am. Chem. Soc.*, 2019, **141**, 849–857.

31 Z. Dong, L. Feng, Y. Chao, Y. Hao, M. Chen, F. Gong, X. Han, R. Zhang, L. Cheng and Z. Liu, Amplification of tumor oxidative stresses with liposomal Fenton catalyst and glutathione inhibitor for enhanced cancer chemotherapy and radiotherapy, *Nano Lett.*, 2019, **19**, 805–815.

32 Z. Dong, L. Feng, Y. Hao, M. Chen, M. Gao, Y. Chao, H. Zhao, W. Zhu, J. Liu, C. Liang, Q. Zhang and Z. Liu, Synthesis of hollow biomineralized $CaCO_3$-polydopamine nanoparticles for multimodal imaging-guided cancer photodynamic therapy with reduced skin photosensitivity, *J. Am. Chem. Soc.*, 2018, **140**, 2165–2178.

33 L. Chen, Z. Lin, L. Liu, X. Zhang, W. Shi, D. Ge and Y. Sun, Fe^{2+}/Fe^{3+} ions chelated with ultrasmall polydopamine nanoparticles induce ferroptosis for cancer therapy, *ACS Biomater. Sci. Eng.*, 2019, **5**, 4861–4869.